Hyperspectral remote sensing for shallow waters. I. A semianalytical model

Zhongping Lee, Kendall L. Carder, Curtis D. Mobley, Robert G. Steward, and Jennifer S. Patch

For analytical or semianalytical retrieval of shallow-water bathymetry and/or optical properties of the water column from remote sensing, the contribution to the remotely sensed signal from the water column has to be separated from that of the bottom. The mathematical separation involves three diffuse attenuation coefficients: one for the downwelling irradiance (K_d), one for the upwelling radiance of the water column (K_u^C), and one for the upwelling radiance from bottom reflection (K_u^B). Because of the differences in photon origination and path lengths, these three coefficients in general are not equal, although their equality has been assumed in many previous studies. By use of the Hydrolight radiative-transfer numerical model with a particle phase function typical of coastal waters, the remote-sensing reflectance above (R_{rs}) and below (r_{rs}) the surface is calculated for various combinations of optical properties, bottom albedos, bottom depths, and solar zenith angles. A semianalytical (SA) model for r_{rs} of shallow waters is then developed, in which the diffuse attenuation coefficients are explicitly expressed as functions of in-water absorption (a) and backscattering (b_b). For remote-sensing inversion, parameters connecting R_{rs} and r_{rs} are also derived. It is found that r_{rs} values determined by the SA model agree well with the exact values computed by Hydrolight ($\sim$3% error), even for Hydrolight r_{rs} values calculated with different particle phase functions. The Hydrolight calculations included b_b/a values as high as 1.5 to simulate high-turbidity situations that are occasionally found in coastal regions. © 1998 Optical Society of America

OCIS codes: 010.0010, 280.0280.

1. Introduction

Single- or quasi-single-scattering theory[1] or numerical simulations suggest that subsurface upwelling signals (S_{US-}, see Section 8 for symbols used in this text) can be approximated as a sum of contributions from the water column and from the bottom:[2–6]

$$S_{US} \approx S_{US}^{dp}[1 - \exp(-2KH)] + S_{US}^B \exp(-2KH). \tag{1}$$

Here S_{US} can designate either the subsurface upwelling radiance (L_{u-}), the subsurface irradiance reflectance (R), or the subsurface remote-sensing reflectance (r_{rs}); we use subsurface to mean just below the air–water surface. S_{US}^{dp} is for optically deep waters, whereas S_{US}^B is for the upwelling signals just above the bottom. H is the depth of the bottom. K is usually described as an effective attenuation coefficient.[2–4,6,7] The first term on the right side of approximation (1) is the water-column contribution, although in some studies this term was replaced by a nearby deep-water signal.[2,4,7,8] The second term is the bottom contribution.

Because the effective attenuation coefficient is ambiguous and hard to determine from remotely measured data, and because the diffuse attenuation coefficient for downwelling light is not generally equal to the diffuse attenuation coefficients for upwelling light, a more general expression for subsurface remote-sensing reflectance, defined as the ratio of upwelling radiance (L_{u-}) to downwelling irradiance (E_{d-}) evaluated just below the surface, is

$$r_{rs} \approx r_{rs}^{dp}\{1 - A_0 \exp[-(K_d + K_u^C)H]\} + A_1\rho$$
$$\times \exp[-(K_d + K_u^B)H], \tag{2}$$

where r_{rs}^{dp} is the r_{rs} value for optically deep waters, K_d is the vertically averaged diffuse attenuation coefficient for downwelling irradiance, K_u^C is the vertically averaged diffuse attenuation coefficient for upwelling radiance from water-column scattering, and K_u^B is the vertically averaged diffuse attenuation coefficient for upwelling radiance from bottom reflectance. ρ is the bottom irradiance reflectance, and the bottom is assumed to be a Lambertian reflector.

We introduce two additional factors into approximation (2): A_0 and A_1. According to quasi-single-scattering theory[1], A_0 would be 1.0 and A_1 would be $1/\pi$ for a Lambertian bottom. However, we want to determine values for A_0 and A_1 from the exact numerical simulations to make the proposed approximation (2) as accurate as possible.

If we define

$$\alpha \equiv a + b_b, \tag{3}$$

then any diffuse attenuation coefficient K can be related to α through an appropriate distribution function (D) (Ref. 9):

$$K = D\alpha. \tag{4}$$

In particular,

$$K_d = D_d\alpha, \quad K_u^C = D_u^C\alpha, \quad K_u^B = D_u^B\alpha, \tag{5}$$

which allows us to rewrite approximation (2) as

$$r_{rs} \approx r_{rs}^{dp}\{1 - A_0 \exp[-(D_d + D_u^C)\alpha H]\}$$
$$+ A_1\rho \exp[-(D_d + D_u^B)\alpha H]. \tag{6}$$

Note that α is an inherent optical property.[9] Thus all the variability in the K's associated with the directional structure of the light field is now transferred to the distribution functions (D).

In many previous remote-sensing applications it was assumed that $D_d = D_u^C = D_u^B =$ a constant,[2,4,7] which is equivalent to using the same attenuation coefficient for downwelling and upwelling light. However, studies of the subsurface light field[1,10] suggest that in general $D_d \neq D_u^C \neq D_u^B \neq$ constant, and that the D's vary with the inherent optical properties of the water column. Incorrect assumptions for the values of the D's will cause errors in water-depth derivations. To improve remote sensing of shallow-water bathymetry, for example, we need to more accurately determine how D varies with in-water optical properties.

Our goal in this study is to develop a simple, explicitly invertable, analytical formula for remote-sensing reflectance for homogeneous waters. To achieve this, the Hydrolight numerical model[11,12] was used to compute remote-sensing reflectance above the surface [R_{rs}, the ratio of water-leaving radiance (L_w) to downwelling irradiance (E_{d+}) just above the surface] and remote-sensing reflectance below the surface (r_{rs}) for a series of water, bottom type, and depth parameters. From these calculated r_{rs} values, parameterizations of D were empirically derived, and a semianalytical (SA) model was developed for r_{rs} of deep and shallow waters. This SA model is explicitly invertable for the calculation of depth and the optical properties of the water column, whereas Hydrolight is strictly a numerical, forward model and is therefore not explicitly invertable.

Although it would be preferable to develop our SA model using an extensive data set of actual observations, data sets covering the needed range of environmental conditions do not exist. Hydrolight gives us a controlled environment in which pseudodata can be generated for any desired environmental conditions. Any SA model based on numerically generated data must of course be tested with actual data whenever the opportunity arises.

2. Semianalytical Model for r_{rs}

A. Deep-Water Formulation
Defining

$$u \equiv b_b/(a + b_b), \tag{7}$$

r_{rs}^{dp} can be expressed as in Gordon et $al.$[13] and Morel and Gentili[14] as

$$r_{rs}^{dp} \approx gu, \tag{8}$$

with g itself expressed as a function of u:

$$g \approx g_0 + g_1 u^{g2}. \tag{9}$$

B. Shallow-Water Formulation
To further simplify the SA model, we assume that[15]

$$D_d \approx 1/\cos(\theta_w),$$

where θ_w is the subsurface solar zenith angle, and we keep D_d as a spectral constant. We thus attribute all the variations of the D's in approximation (6) to D_u^C and D_u^B only. However, we must keep in mind that both D_d and D_u do vary with b_b and a, which means that part of the variations of D_u^C and D_u^B versus b_b and a are a result of that for D_d. For remote-sensing applications, it is not necessary to separate D_u^C and D_u^B from D_d, because approximation (6) depends only on the sum of D_d and D_u^C and the sum of D_d and D_u^B. For in-water K_d studies, however, it is necessary to know the relationship between D_d versus b_b and a, as in Kirk.[10]

A Kirk[10] K type of formula,

$$D_u = D_0(1 + D_1 u)^{0.5} \tag{10}$$

is applied to describe the relationships between D_u and $b_b/(a + b_b)$, where D_0 and D_1 are constant coefficients to be determined.

Table 1. Environmental Input used in the Hydrolight Simulations

Variable	Inputs
Solar zenith angle	0°, 30°, 60°
Particle phase function	Petzold average particle
Chlorophyl a [chl-a] ($mg\ m^{-3}$)	0.4, 1.0, 2.0, 5.0
$a_g(440)$ (m^{-1})	0.05, 0.1, 0.3
B	0.3, 1.0, 5.0
ρ	0, 0.1, 0.3, 1.0
H (m)	0.5, 1, 3, 8, 16, 32, infinite
λ (nm)	400–700, every 20 nm

Table 2. Parameters for the Empirical $a_\phi(\lambda)$ Simulation by Eq. (12)[a]

Wavelength	$a_0(\lambda)$	$a_1(\lambda)$
390	0.5813	0.0235
400	0.6843	0.0205
410	0.7782	0.0129
420	0.8637	0.006
430	0.9603	0.002
440	1.0	0
450	0.9634	0.006
460	0.9311	0.0109
470	0.8697	0.0157
480	0.789	0.0152
490	0.7558	0.0256
500	0.7333	0.0559
510	0.6911	0.0865
520	0.6327	0.0981
530	0.5681	0.0969
540	0.5046	0.09
550	0.4262	0.0781
560	0.3433	0.0659
570	0.295	0.06
580	0.2784	0.0581
590	0.2595	0.054
600	0.2389	0.0495
610	0.2745	0.0578
620	0.3197	0.0674
630	0.3421	0.0718
640	0.3331	0.0685
650	0.3502	0.0713
660	0.561	0.1128
670	0.8435	0.1595
680	0.7485	0.1388
690	0.389	0.0812
700	0.136	0.0317
710	0.0545	0.0128
720	0.025	0.005

[a]Taken from Lee.[22]

Our proposed SA formula for deep and shallow water r_{rs} is then

$$r_{\mathrm{rs}} = (g_0 + g_1 u^{g_2})u\left(1 - A_0 \exp\left\{-\left[\frac{1}{\cos(\theta_w)}\right.\right.\right.$$
$$\left.\left.\left. + D_0(1 + D_1 u)^{0.5}\right]\alpha H\right\}\right) + A_1\rho \exp\left\{-\left[\frac{1}{\cos(\theta_w)}\right.\right.$$
$$\left.\left. + D_0{}'(1 + D_1{}'u)^{0.5}\right]\alpha H\right\}. \tag{11}$$

The values of $g_{0,1,2}$, $A_{0,1}$, $D_{0,1}$, and $D_{0,1}{}'$ are derived from Hydrolight-generated r_{rs} values.

3. Computer Simulations of R_{rs} and r_{rs}

Hydrolight version 3.0 (Ref. 16) was employed for the generation of nadir-viewing R_{rs} and r_{rs} values. We chose the Hydrolight radiative transfer numerical model[11,12] for our simulations for several reasons:

(1) Hydrolight has been used by many researchers and for many applications (e.g., Refs. 17–19) and consequently has been extensively debugged and validated.

(2) Hydrolight is much faster than Monte Carlo simulation for problems involving the upwelling radiance,[11] as in the present study. Moreover, Hydrolight computes all radiances with the same accuracy, whereas Monte Carlo simulations contain much more statistical noise in upwelling radiances than in downwelling[11,12] because of the fewer number of backscattered solar photons. Hydrolight does not have any statistical noise at all arising from the solution of the radiative transfer equation.

(3) Hydrolight contains the needed physics (wind-blown surfaces, finite or infinite bottom depth, spectral dependence of inherent optical properties, all orders of multiple scattering within the water and between the water surface and bottom, etc.). Not all models now in use contain all the needed features.

Table 1 summarizes the inputs used in the Hydrolight simulations. For all calculations, a wind speed of 5 m/s was used, and the water body was assumed homogeneous with a refractive-index value of 1.34. Above-surface downwelling spectral irradiances were computed by the model of Gregg and Carder,[20] using solar zenith angles of 0°, 30°, and 60°. Both clear and cloudy skys were simulated.

The total absorption coefficient is expressed as a sum of the absorption coefficients for pure water, phytoplankton pigments, and gelbstoff. Absorption values for pure water are taken from Pope and Fry,[21] whereas absorption for phytoplankton pigments and gelbstoff were modeled with simple bio-optical models, which give a realistic simulation of a variety of waters.

The phytoplankton pigment absorption coefficient is simulated using the empirical model in Lee,[22] expressed as

$$a_\phi(\lambda) = \{(a_0(\lambda) + a_1(\lambda)\ln[a_\phi(440)]\}a_\phi(440). \tag{12}$$

Values for $a_0(\lambda)$ and $a_1(\lambda)$ have been already empirically determined and are shown in Table 2. Thus, given an $a_\phi(440)$ value, an $a_\phi(\lambda)$ spectrum is constructed with Eq. (12). As can be seen in Fig. 1, this approach allows the $a_\phi(\lambda)$ curvature to change with $a_\phi(440)$, which is consistent with field observations, at least to the first order.

In the Hydrolight calculations, $a_\phi(440)$ can be an input by itself or can be linked to another parameter
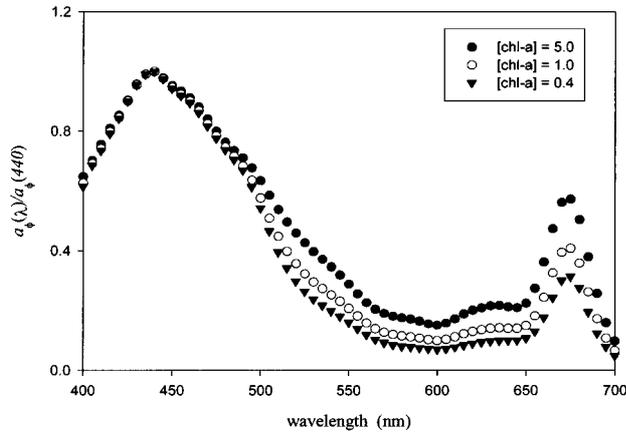
Fig. 1. Examples of simulated pigment absorption coefficients as computed by Eqs. (12) and (13) for three different chlorophyll a concentrations; curves are normalized to 1.0 at 440 nm to show the curvature dependence on [chl-a].
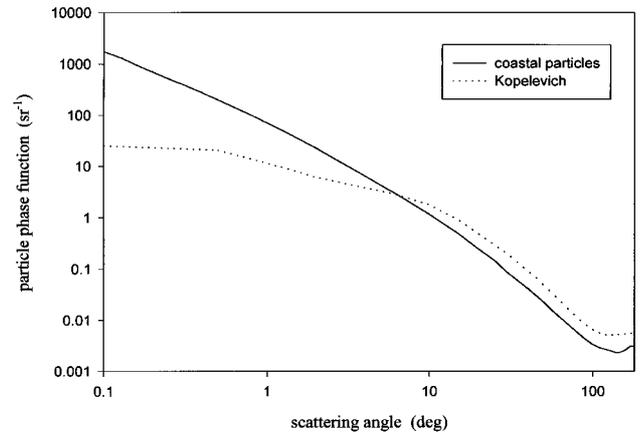

Fig. 2. Particle phase functions used in the Hydrolight calculations. The solid curve represents the calculations used in the parameter determination; the dashed curve represents the calculations used in the test.

such as chlorophyll a concentration ([chl-a]). To be consistent with the calculations of other researchers and to keep the input values for absorption and scattering within the appropriate ranges, we used [chl-a] as input to determine the $a_\phi(440)$ and $b_p(550)$ values (see below). $a_\phi(440)$ is determined by[23]

$$a_\phi(440) = 0.06[\text{chl-a}]^{0.65}. \qquad (13)$$

Gelbstoff absorption is expressed as in Bricaud *et al.*[24]:

$$a_g(\lambda) = a_g(440)\exp[-0.014(\lambda - 440)], \qquad (14)$$

with $a_g(440)$ an independent variable (see Table 1). The total scattering coefficient is expressed as a sum of the scattering coefficients for pure seawater and particles. Scattering coefficients for pure seawater come from Morel,[25] whereas scattering coefficients for particles come from the model of Gordon and Morel[26]:

$$b_p(\lambda) = B[\text{chl-a}]^{0.62}550/\lambda. \qquad (15)$$

Here B is an empirical value, which was 0.3 in Gordon and Morel.[26] We used B values of 0.3, 1.0, and 5.0 to simulate a range from normal to highly turbid coastal waters.

Most simulations used the Petzold-type average particle phase function described in Mobley *et al.*[11] and in Table 3.10 of Ref. 12. This phase function has a b_{bp}/b_p ratio of 1.9%. This phase function is shown in Fig. 2 along with a more highly backscattering (b_{bp}/b_p ratio of 3.7%) Kopelevich phase function[12] for suspended sediments, which are discussed in Section 5 below. The pure seawater scattering was treated as a separate component with a Rayleigh-like phase function.[11,12] The ratio of pure seawater to particle scattering varied with the particle scattering coefficient.

A spectrally constant bottom albedo ρ was used in the calculations; ρ values of 0, 0.1, 0.3, and 1.0 were used in the simulations. Although the bottom reflectance was taken to be independent of wavelength,

the water-column inherent optical properties were wavelength dependent.

4. Results and Discussion

A. Deep Waters

As discovered in Gordon *et al.*[13] and Morel and Gentili[14] through Monte Carlo simulations, nadir-viewing r_{rs} is almost independent of solar zenith angle [see Fig. 3 for r_{rs} values versus $b_b/(a + b_b)$ for the three Sun angles]. This result is different from that for subsurface irradiance reflectance (R, ratio of upwelling irradiance to downwelling irradiance), which is a stronger function of solar zenith angle.[10,27,28] Detailed discussions regarding this difference can be found in Morel and Gentili.[14]

Figure 4 demonstrates the changes in r_{rs} values with b_b/a. Similar to earlier Monte Carlo studies,[13,14] it was found that r_{rs} increases with ratios $b_b/(a + b_b)$ or b_b/a, but at a different rate. r_{rs} quickly increases with $b_b/(a + b_b)$, especially when
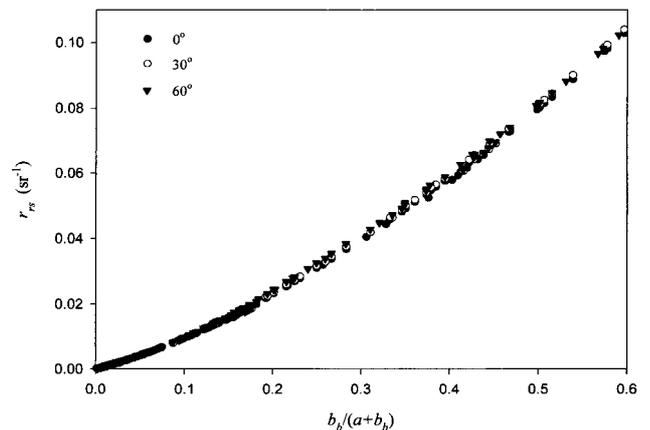

Fig. 3. Dependence of deep water r_{rs} on $b_b/(a + b_b)$, as simulated by Hydrolight. The simulations include various environmental conditions as shown in Table 1.
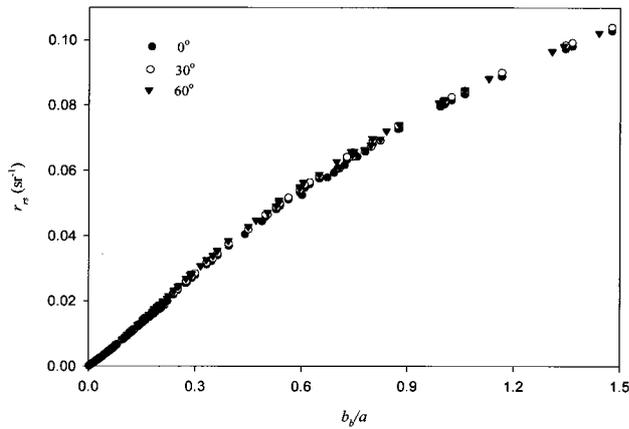
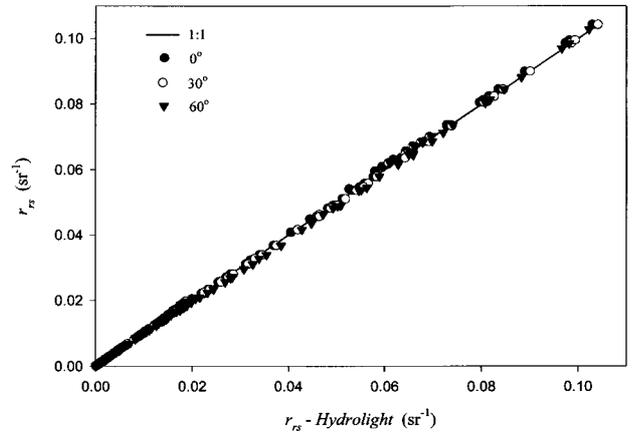Fig. 4. Dependence of deep water r_{rs} on b_b/a.

Fig. 5. Comparison of deep water r_{rs} values as computed by Hydrolight and by the SA model. Values for the different solar zenith angles are identified.

the ratio is relatively large. However, r_{rs} increases more slowly with b_b/a, especially for $b_b/a > 0.3$, in a manner similar to that found by Jerome *et al.*[29] and Kirk[10] for subsurface irradiance reflectance.

The values of the empirical parameters $g_{0,1,2}$ in Eq. (11) were determined first, by use of Hydrolight simulations for infinitely deep water. r_{rs} values computed by Hydrolight were compared with the values given by approximations (8) and (9) as $g_{0,1,2}$ were systematically varied. The best-fit set of g values was determined by minimizing the following quantity as in Gordon and Boynton[30]:

$$\delta = \text{mean}\left|\ln\left(\frac{r_{rs}{}^s}{r_{rs}{}^H}\right)\right|,$$

where $r_{rs}{}^s$ is a SA model simulated value and $r_{rs}{}^H$ is a Hydrolight-calculated value. The mean here is based on all Hydrolight calculations, i.e., over all sets of inherent optical properties and sky conditions and over all wavelengths. The resulting best-fit set of g parameters are $g_0 \approx 0.070$, $g_1 \approx 0.155$, and $g_2 \approx 0.752$. Therefore

$$r_{rs}{}^{dp} \approx (0.070 + 0.155u^{0.752})u. \qquad (16)$$

Figure 5 presents the deep-water r_{rs} values as calculated by Hydrolight and as obtained from approximation (16); the error ($e^\delta - 1$) is approximately 1%. Figure 6 shows examples of r_{rs} spectra as computed by Hydrolight and by approximation (16); the different curves are for different optical property values. As expected, the r_{rs} values from both calculation methods agree very well. Note that approximation (16) includes data with both low and high u values, i.e., data for a wide range of inherent optical properties for waters.

We could also try to express $r_{rs}{}^{dp}$ as a simple function of b_b/a, instead of $b_b/(a + b_b)$, as has been done in many studies of subsurface irradiance reflectance.[10,22,28,29,31] For coastal waters, however, one expression cannot adequately cover both small and large b_b/a situations.[10,29] Two or more expressions with different g parameters for different b_b/a ranges have to be applied.[29]

Gordon *et al.*[13] found through Monte Carlo simulation that, for most oceanic waters, $r_{rs}{}^{dp}$ can be expressed as

$$r_{rs}{}^{dp} \approx (0.0949 + 0.0794u)u. \qquad (17)$$

Morel and Gentili[14] found that for case 1 waters,[32]

$$r_{rs}{}^{dp} \approx 0.0922b_b/a,$$

which is equivalent to

$$r_{rs}{}^{dp} \approx \frac{0.0922}{1 - u}u. \qquad (18)$$

Figure 7 compares approximations (16), (17), and (18) for deep-water remote-sensing reflectance. We can see that for u less than 0.3 (b_b/a less than ~0.4), the three expressions provide very close $r_{rs}{}^{dp}$ values. This agreement demonstrates that the three expressions are all consistent with each other, even though they were developed through different computer simulations. The slightly smaller $r_{rs}{}^{dp}$ values found using approximation (16) rather than using approximation (17) for u values less than 0.05 (see inset in Fig. 7) may be due to technical differences
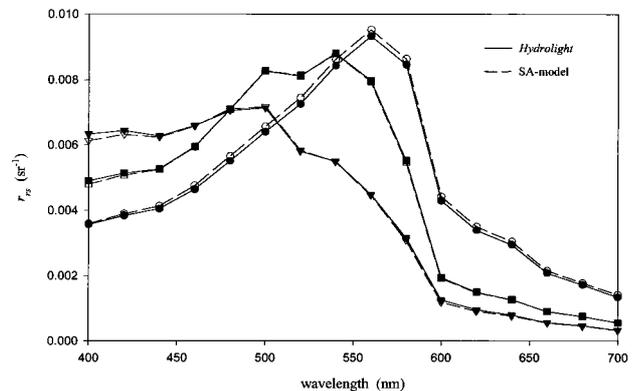

Fig. 6. Examples of r_{rs} spectra as computed by Hydrolight (filled symbols) and by the SA model (open symbols).
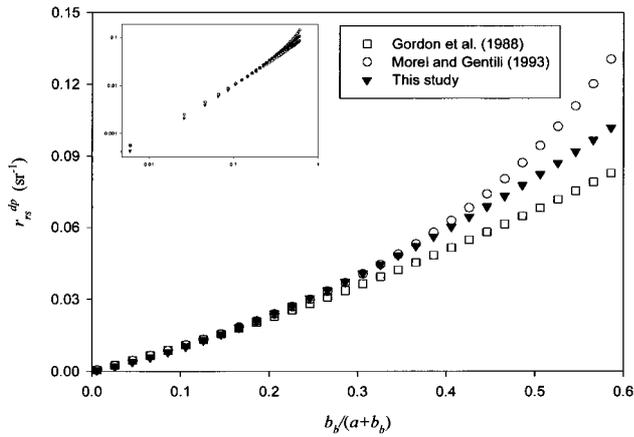
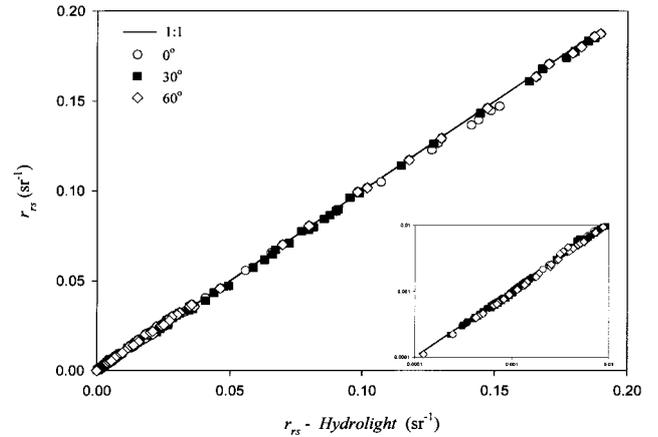Fig. 7. Comparison of r_{rs}^{dp} values as determined by three different expressions.

Fig. 8. Comparison of shallow water r_{rs} values as computed by Hydrolight and by the SA model for different solar zenith angles.

between the Hydrolight and Monte Carlo simulations as pointed out in Mobley *et al.*,[11] especially for the calculation of upwelling radiance.[11] This difference of roughly 10% is also within the error bounds of Gordon *et al.*[13] Because the expressions of Gordon *et al.*[13] and Morel and Gentili[14] were developed for open-ocean applications, extrapolation of approximations (17) and (18) to waters with u values larger than 0.3 may not be appropriate. Therefore we suggest that approximations (17) and (18) are consistent for open-ocean waters, and that approximation (16) extends those expressions to the realm of turbid coastal waters. A test using a more mineral-rich expression for the particle phase function shows only a small effect on the SA model performance (see Section 5).

B. Shallow Waters

The remaining parameters $A_{0,1}$, $D_{0,1}$, and $D_{0,1}'$ were simultaneously determined by comparing Hydrolight-calculated r_{rs} values with those given by Eq. (11) and minimizing the δ value as above. The resulting best-fit parameter values are

$$A_0 \approx 1.03, \quad A_1 \approx 0.31,$$

$$D_u^C \approx 1.2(1 + 2.0u)^{0.5}, \tag{19}$$

$$D_u^B \approx 1.1(1 + 4.9u)^{0.5}. \tag{20}$$

Therefore Eq. (11) takes the specific form

$$
\begin{aligned}
r_{rs} \approx & (0.070 + 0.155u^{0.752})u\left(1 - 1.03\exp\left\{-\left[\frac{1}{\cos(\theta_w)}\right.\right.\right. \\
& \left.\left. + 1.2(1 + 2.0u)^{0.5}\right]\alpha H\right\}\right) \\
& + 0.31\rho\exp\left\{-\left[\frac{1}{\cos(\theta_w)} + 1.1\right.\right. \\
& \left.\left. \times (1 + 4.9u)^{0.5}\right]\alpha H\right\}. \tag{21}
\end{aligned}
$$

Figure 8 compares r_{rs} values calculated by Hydrolight versus those determined by approximation (21)

for shallow waters; the error is approximately 3%. Although reasonably close agreement is to be anticipated because the SA model parameters were determined with Hydrolight data, ±3% agreement nevertheless indicates the excellent predictive power of the SA model over a wide range of optical environments. Note that approximation (21) predicts r_{rs} given only the absorption and backscattering properties of the water column, the solar zenith angle, the water depth, and the bottom reflectance. This is the desired SA model for r_{rs}.

We did not try to fit the Hydrolight r_{rs} values of shallow, black-bottom environments to derive A_0 and $D_{0,1}$ only, because such r_{rs} values lack the interaction between photons scattered by the water column and by the bottom.

The values for A_0 and A_1 are almost identical (~3% difference) to their values suggested by use of single- or quasi-single-scattering theory[2–6,8,33] (recall Section 1), which suggests that the SA model and the empirically derived values are consistent with theory. The small difference found may be due to the fact that approximation (6) is a simplified expression based on use of quasi-single-scattering theory. It therefore cannot be expected to perfectly describe a complicated shallow-water environment. We must keep in mind that the simple truncation of approximation (1) [the term in the bracket on the right side; or approximation (2) with $A_0 = 1.0$] for water columns with black bottoms only accounts to the first order for the reduction of the number of particles making contributions to r_{rs}. A black-bottom-truncated water column, however, reduces not only the number of scattering particles, but also the multiple-scattering probabilities, especially for cases with higher b_b/a. Also, as Gordon and Brown[34] indicated, it is not true that part of the photons will just hit bottom while the other part will not. Thus the slight departure of A_0 from 1.0 and of A_1 from $1/\pi$ for the current calculation reflects in part the difference between approximation (6) and the exact Hydrolight r_{rs} values. Simply setting A_0 to 1.0 and A_1 to $1/\pi$ would require the values of D_1 in Eq. (11) be negative
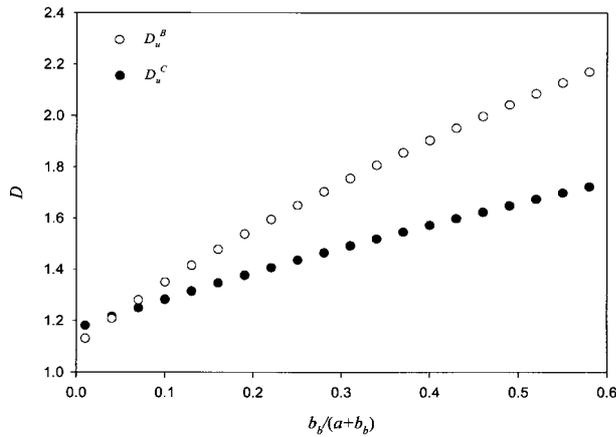
Fig. 9. Dependence of distribution functions on $b_b/(a + b_b)$.

Fig. 11. Comparison of deep water r_{rs} values computed by Hydrolight with the Kopelevich phase function of Fig. 2 with r_{rs} values given by the SA model, which is based on the coastal particle phase function of Fig. 2.

to fit all the Hydrolight-generated r_{rs} values. This suggests that $D_u{}^C$ will be smaller for high b_b/a waters, which is contrary to the findings of Kirk.[10] To force A_0 to 1.0, A_1 to $1/\pi$, and allow appropriate values for $D_{0,1}$ and $D_{0,1}{}'$, a more complicated expression than approximation (6) [or Eq. (11)] is required. We therefore choose to retain the best-fit values of A_0 and A_1 in approximation (21), so as to provide the SA model greater possible applicability.

Figure 9 shows the behavior of $D_u{}^C$ and $D_u{}^B$ for u less than 0.6 (b_b/a less than ~1.5). The ranges for $D_u{}^C$ and $D_u{}^B$ are 1.2–1.7 and 1.1–2.2, respectively. This indicates that the paths of photons reflected by the bottom are longer than those of photons scattered by the water column, especially for waters of high b_b/a. Earlier, Lee et al.[5] empirically suggested an average value of 1.5 for $D_u{}^B$; this average is consistent with the finding here.

Figure 10 shows the ratios of r_{rs} at two wavelengths as a function of H; note that the absorption coefficient is much smaller at λ_1 than at λ_2. It should be noted that for some combinations of water-column optical properties and bottom albedo, there are two depths that correspond to the same r_{rs} ratio. Only when the water is very clear and shallow, i.e.,
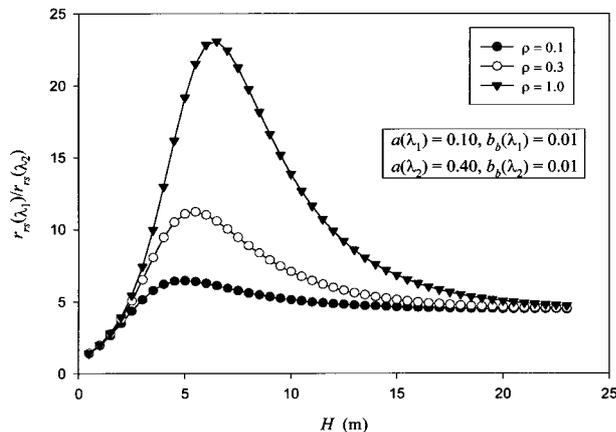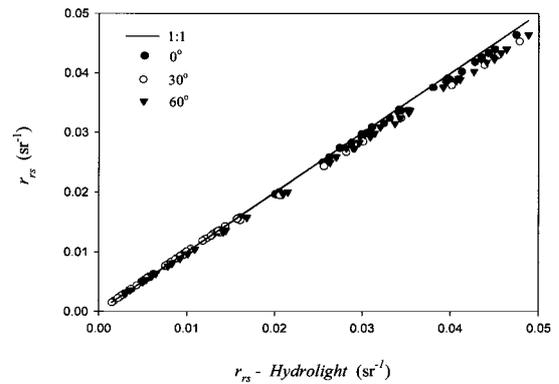
when the water-column contributions are negligible, do spectral ratios of r_{rs} become almost independent of the bottom albedo values. These observations suggest that use of just two wavelength channels may be insufficient to retrieve the bottom depth even when the optical properties of the water column and the bottom albedo are known. For shallow-water remote sensing, additional channels are almost certainly required for the retrieval of both depth and optical properties of the water column.

5. Test with a Different Particle Phase Function

To evaluate the validity of approximations (16) and (21) for a variety of water environments, another r_{rs} data set was generated by use of a different particle phase function as input to Hydrolight. This particle phase function is given by the formula of Kopelevich[12] and has a b_{bp}/b_p ratio of 3.7%, which is approximately a factor of 2 larger than the particle phase function used in the parameter development (recall Fig. 2). The particle phase function is assumed to be the same for all wavelengths. Figures 11 and 12 show r_{rs} values computed by Hydrolight with the Kopelevich phase function versus those determined
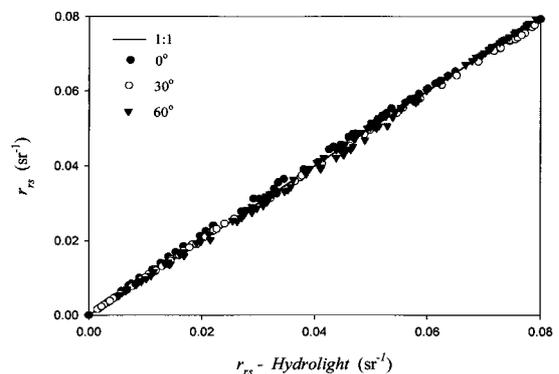

Fig. 10. Ratios of r_{rs} at two wavelengths as a function of bottom depth and reflectance.

Fig. 12. Comparison of shallow water r_{rs} values computed by Hydrolight with the Kopelevich phase function of Fig. 2 with r_{rs} values given by the SA model, which is based on the coastal particle phase function of Fig. 2.

with approximations (16) and (21) for deep and shallow waters, respectively. As can be seen, the r_{rs} values calculated by both methods still agree quite well with each other (approximately 3% error for both deep and shallow situations). These results suggest that there is a potential for wide application of approximations (16) and (21) to water environments with considerably different scattering properties.

6. Across the Water–Air Interface

Approximation (21) provides only the r_{rs} values below the surface, but a remote sensor measures above-surface values. Therefore the relation between R_{rs} and r_{rs} needs to be known. From Mobley[12] and Gordon et al.,[13] there is

$$R_{rs} = \frac{L_w}{E_{d+}} = \frac{t_- t_+}{n^2} \frac{R}{Q(1 - \gamma R)},$$ (22)

where t_- is the radiance transmittance from below to above the surface, t_+ is the irradiance transmittance from above to below the surface, n is the refractive index of water, R is the subsurface irradiance reflectance, γ is the water-to-air internal reflection coefficient, and Q is the ratio of E_{u-} to L_{u-}.

Noting that

$$r_{rs} = \frac{L_{u-}}{E_{d-}} = \frac{R}{Q},$$ (23)

and defining

$$\zeta = \frac{t_- t_+}{n^2}$$

as the water-to-air radiance-divergence factor, we can write

$$R_{rs} = \frac{\zeta r_{rs}}{1 - \Gamma r_{rs}},$$ (24)

where $\Gamma = Q \gamma$. Note that Eq. (24) is exact. The denominator $1 - \Gamma r_{rs}$ accounts for the effects of internal reflection from water to air. Although this internal-reflection term is often ignored, especially for open-ocean waters, we retain it in the present study because r_{rs} can be quite large for turbid or shallow waters. For remote-sensing applications, the values of ζ and Γ in Eq. (24) need to be determined. By comparing the Hydrolight-generated R_{rs} and r_{rs} values, it is found that $\zeta \approx 0.518$ and $\Gamma \approx 1.562$. This value of ζ is consistent with the analysis in Gordon et al.[13] Recall that Γ is the product of γ and Q. If γ is approximately 0.48 (Lyzenga[35] and Ref. 13), then Q has a value of 3.25, which is consistent with the nadir values seen in Morel and Gentili.[14] For other view angles, values of ζ and Γ may be slightly different. Thus Eq. (24) takes the specific form

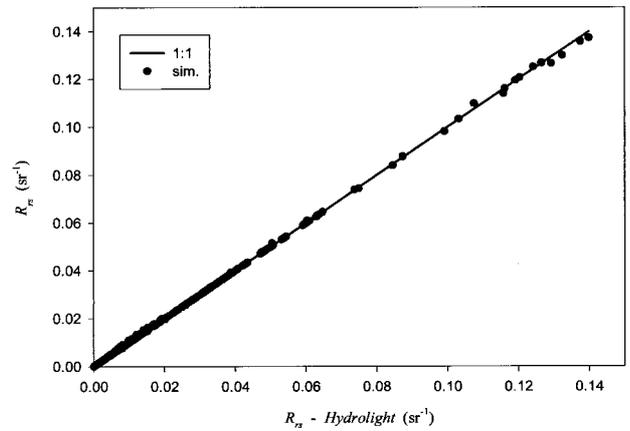$$R_{rs} \approx \frac{0.518 r_{rs}}{1 - 1.562 r_{rs}}.$$ (25)

Fig. 13. Comparison of R_{rs} values computed by Hydrolight and by approximation (25).

Figure 13 shows R_{rs} as calculated by approximation (25) and by Hydrolight.

If we consider the idealized case of perfectly clear water ($u = 0$), a perfectly reflecting bottom ($\rho = 1.0$) and infinitesimally deep water ($H = 0$), approximation (21) provides an r_{rs} value of ~0.31 sr^{-1}, whereas approximation (25) also results in $R_{rs} \approx 0.31$ sr^{-1}. These results are consistent with Hydrolight-calculated values. However, if the internal reflection term [the denominator of approximation (25)] had been omitted, $R_{rs} \approx 0.16$ sr^{-1} from approximation (25), which is in serious error. These results clearly show that it is necessary to retain the internal reflection term in approximation (25) when working in shallow or turbid waters, and that the above values for ζ and Γ are appropriate.

7. Summary

By use of the Hydrolight radiative transfer numerical model with inherent optical properties typical of coastal waters, R_{rs} and r_{rs} values were calculated for both deep and shallow waters. The calculated r_{rs} values were used to determine the empirical parameters for a SA model for r_{rs}. All model parameters are explicitly determined as functions of a and b_b. The resulting deep-water r_{rs} expression is consistent with earlier Monte Carlo studies for deep, low-scattering waters and has potential for application to turbid waters with high b_b/a. Because the SA model explicitly includes bottom effects, it provides a basis for analytical inversion of r_{rs} spectra to obtain shallow-water properties such as depth and bottom albedo, as well as water-column absorption and back-scatter. The SA model predictions were tested against r_{rs} values calculated by Hydrolight using two different particle phase functions, and it was found that the r_{rs} values from both Hydrolight and the SA model agree with each other quite well (approximately 3% error for both deep- and shallow-water r_{rs} values). This indicates that predictions made by the SA model are not strongly dependent on the (generally unknown) scattering phase function. Therefore the SA model can be used to accurately and quickly

predict the r_{rs} spectrum of various shallow waters, in contrast to time-consuming Monte Carlo or Hydrolight calculations. Also, parameters connecting R_{rs} and r_{rs} are also derived from Hydrolight-generated values. This bodes well for rapid model inversions of high-resolution, measured, spectral R_{rs} data sets to obtain values of H, ρ, $a(\lambda)$, and $b_b(\lambda)$. Knowing these values may in turn enable the recovery of quantities such as chlorophyll a, gelbstoff, and suspended particulate matter concentrations from empirical relationships with $a(\lambda)$ and $b_b(\lambda)$.

8. Symbols Used in Text

a_w absorption coefficient of pure seawater, m^{-1};
a_ϕ absorption coefficient of phytoplankton pigments, m^{-1};
a_g absorption coefficient of gelbstoff, m^{-1};
a absorption coefficient of the total, m^{-1};
B an empirical value to describe particle scattering coefficient;
b scattering coefficient, m^{-1};
b_b backscattering coefficient, m^{-1};
b_p scattering coefficient of suspended particles, m^{-1};
b_{bp} backscattering coefficient of suspended particles, m^{-1};
D distribution function;
E_d downwelling irradiance, $W/nm/m^2$;
$E_{d+,d-}$ downwelling irradiance just above $(+)$ or below $(-)$ the surface, $W/nm/m^2$;
E_u upwelling irradiance, $W/nm/m^2$;
f water-to-air divergence factor;
H bottom depth, m;
K diffuse attenuation coefficients, m^{-1};
L_{u-} subsurface upwelling radiance, $W/m^2/nm/sr$;
L_w water-leaving radiance, $W/m^2/nm/sr$;
n refractive index of water;
Q ratio of subsurface upwelling irradiance to upwelling radiance, sr;
r_{rs} subsurface remote-sensing reflectance, sr^{-1};
r_{rs}^{dp} subsurface remote-sensing reflectance for optically deep waters, sr^{-1};
R subsurface irradiance reflectance;
R_{rs} above-surface remote-sensing reflectance, sr^{-1};
S_{US} subsurface upwelling signal;
$t_{+,-}$ diffuse transmittance from above (below) to below (above) the surface;
[chl-a] chlorophyll a concentration, mg/m^3;
α attenuation coefficient ($= a + b_b$), m^{-1};
ρ bottom albedo;
θ_w subsurface solar zenith angle, rad;
γ water-to-air internal reflection.

References

1. H. R. Gordon, O. B. Brown, and M. M. Jacobs, "Computed relationship between the inherent and apparent optical properties of a flat homogeneous ocean," Appl. Opt. **14,** 417–427 (1975).
2. D. R. Lyzenga, "Passive remote-sensing techniques for mapping water depth and bottom features," Appl. Opt. **17,** 379–883 (1978).
3. W. D. Philpot, "Bathymetric mapping with passive multispectral imagery," Appl. Opt. **28,** 1569–1578 (1989).
4. N. T. O'Neill and J. R. Miller, "On calibration of passive optical bathymetry through depth soundings analysis and treatment of errors resulting from the spatial variation of environmental parameters," Int. J. Remote Sensing **10,** 1481–1501 (1989).
5. Z. P. Lee, K. L. Carder, S. K. Hawes, R. G. Steward, T. G. Peacock, and C. O. Davis, "Model for the interpretation of hyperspectral remote-sensing reflectance," Appl. Opt. **33,** 5721–5732 (1994).
6. S. Maritorena, A. Morel, and B. Gentili, "Diffuse reflectance of oceanic shallow waters: influence of water depth and bottom albedo," Limnol. Oceanogr. **39,** 1689–1703 (1994).
7. J. M. Paredes and R. E. Spero, "Water depth mapping from passive remote sensing data under a generalized ratio assumption," Appl. Opt. **22,** 1134–1135 (1983).
8. D. Spitzer and R. W. J. Dirks, "Bottom influence on the reflectance of the sea," Int. J. Remote Sensing **8,** 279–290 (1987).
9. R. W. Preisendorfer, *Hydrologic Optics*, Vol. 1: Introduction, NTIS PB-259 793/8ST (National Technical Information Service, Springfield, Va., 1976).
10. J. T. O. Kirk, "Volume scattering function, average cosines, and the underwater light field," Limnol. Oceanogr. **36,** 455–467 (1991).
11. C. D. Mobley, B. Gentili, H. R. Gordon, Z. Jin, G. W. Kattawar, A. Morel, P. Reinersman, K. Stamnes, and R. H. Stavn, "Comparison of numerical models for computing underwater light fields," Appl. Opt. **32,** 7484–7504 (1993).
12. C. D. Mobley, *Light and Water: Radiative Transfer in Natural Waters* (Academic, New York, 1994).
13. H. R. Gordon, O. B. Brown, R. H. Evans, J. W. Brown, R. C. Smith, K. S. Baker, and D. K. Clark, "A semianalytic radiance model of ocean color," J. Geophys. Res. **93,** 10,909–10,924 (1988).
14. A. Morel and B. Gentili, "Diffuse reflectance of oceanic waters. II. Bidirectional aspects," Appl. Opt. **32,** 6864–6879 (1993).
15. H. R. Gordon, "Can the Lambert-Beer law be applied to the diffuse attenuation coefficient of ocean water?" Limnol. Oceanogr. **34,** 1389–1409 (1989).
16. C. D. Mobley, *Hydrolight 3.0 Users' Guide*, Final Report (SRI International, Menlo Park, Calif., 1995).
17. T. Tyrrell, P. M. Holligan, and C. D. Mobley are preparing the following paper for publication: "Optical impacts of oceanic coccolithophore blooms."
18. J. Berwald, D. Stramski, C. D. Mobley, and D. A. Kiefer are preparing the following paper for publication: "The effect of Raman scattering on the underwater light field."
19. C. D. Mobley and D. Stramski. "Effects of microbial particles on oceanic optics: methodology for radiative transfer modeling and example simulations," Limnol. Oceanogr. **42,** 550–560 (1997).
20. W. W. Gregg and K. L. Carder, "A simple spectral solar irradiance model for cloudless maritime atmospheres," Limnol. Oceanogr. **35,** 1657–1675 (1990).
21. R. Pope and E. Fry, "Absorption spectrum (380-700 nm) of pure waters: II. Integrating cavity measurements," Appl. Opt. **36,** 8710–8723 (1997).

22. Z. P. Lee, "Visible-infrared remote-sensing model and applications for ocean waters," Ph.D. dissertation (Department of Marine Science, University of South Florida, St. Petersburg, Fla., 1994).

23. L. Prieur and S. Sathyendranath, "An optical classification of coastal and oceanic waters based on the specific spectral absorption curves of phytoplankton pigments, dissolved organic matter, and other particulate materials," Limnol. Oceanogr. **26,** 671–689 (1981).

24. A. Bricaud, A. Morel, and L. Prieur, "Absorption by dissolved organic matter of the sea (yellow substance) in the UV and visible domains," Limnol. Oceanogr. **26,** 43–53 (1981).

25. A. Morel, "Optical properties of pure water and pure sea waters," in *Optical Aspects of Oceanography*, N. G. Jerlov and E. S. Nielsen, eds. (Academic, New York, 1974), pp. 1–24.

26. H. R. Gordon and A. Morel, *Remote Assessment of Ocean Color for Interpretation of Satellite Visible Imagery: a Review* (Springer-Verlag, New York, 1983), p. 44.

27. H. R. Gordon, "Dependence of the diffuse reflectance of natural waters on the sun angle," Limnol. Oceanogr. **34,** 1484–1489 (1989).

28. A. Morel and B. Gentili, "Diffuse reflectance of oceanic waters: its dependence on Sun angles as influenced by the molecular scattering contribution," Appl. Opt. **30,** 4427–4438 (1991).

29. J. H. Jerome, R. P. Bukata, and J. E. Burton, "Utilizing the components of vector irradiance to estimate the scalar irradiance in natural waters," Appl. Opt. **27,** 4012–4018 (1988).

30. H. R. Gordon and G. C. Boynton, "Radiance—irradiance inversion algorithm for estimating the absorption and backscattering coefficients of natural waters: homogeneous waters," Appl. Opt. **36,** 2636–2641 (1997).

31. S. Sathyendranath and T. Platt, "Analytical model of ocean color," Appl. Opt. **36,** 2620–2629 (1997).

32. A. Morel and L. Prieur, "Analysis of variations in ocean color," Limnol. Oceanogr. **22,** 709–722 (1977).

33. W. D. Philpot, "Radiative transfer in stratified waters: a single-scattering approximation for irradiance," Appl. Opt. **26,** 4123–4132 (1987).

34. H. R. Gordon and O. B. Brown, "Influence of bottom depth and albedo on the diffuse reflectance of a flat homogeneous ocean," Appl. Opt. **13,** 2153–2159 (1974).

35. D. R. Lyzenga, "Reflectance of a flat ocean in the limit of zero water depth," Appl. Opt. **16,** 282–283 (1977).